Atmosphere **2015**, *6*, 1487-1506; doi:10.3390/atmos6101487

OPEN ACCESS

atmosphere

ISSN 2073-4433

www.mdpi.com/journal/atmosphere

Article

Inland Concentrations of Cl_2 and $ClNO_2$ in Southeast Texas Suggest Chlorine Chemistry Significantly Contributes to Atmospheric Reactivity

Cameron B. Faxon, Jeffrey K. Bean and Lea Hildebrandt Ruiz *

Center for Energy and Environmental Resources, The University of Texas at Austin, Austin, TX 78758, USA; E-Mails: cfaxon1@gmail.com (C.B.F.); jbean15@gmail.com (J.K.B.)

* Author to whom correspondence should be addressed; E-Mail: lhr@che.utexas.edu; Tel.: +1-512-471-1050.

Academic Editor: Armin Sorooshian

Received: 31 August 2015 / Accepted: 8 October 2015 / Published: 14 October 2015

Abstract: Measurements of molecular chlorine (Cl_2), nitryl chloride ($ClNO_2$), and dinitrogen pentoxide (N_2O_5) were taken as part of the DISCOVER-AQ Texas 2013 campaign with a High Resolution Time-of-Flight Chemical Ionization Mass Spectrometer (HR-ToF-CIMS) using iodide (I-) as a reagent ion. $ClNO_2$ concentrations exceeding 50 ppt were regularly detected with peak concentrations typically occurring between 7:00 a.m. and 10:00 am. Hourly averaged Cl_2 concentrations peaked daily between 3:00 p.m. and 4:00 p.m., with a 29-day average of 0.9 ± 0.3 (1σ) ppt. A day-time Cl_2 source of up to 35 ppt·h^{-1} is required to explain these observations, corresponding to a maximum chlorine radical ($Cl^{\bullet}$) production rate of 70 ppt·h^{-1}. Modeling of the Cl_2 source suggests that it can enhance daily maximum O_3 and $RO_2^{\bullet}$ concentrations by 8%–10% and 28%–50%, respectively. Modeling of observed $ClNO_2$ assuming a well-mixed nocturnal boundary layer indicates O_3 and $RO_2^{\bullet}$ enhancements of up to 2.1% and 38%, respectively, with a maximum impact in the early morning. These enhancements affect the formation of secondary organic aerosol and compliance with air quality standards for ozone and particulate matter.

Keywords: ambient observations; air quality; photochemistry; atomic chlorine; molecular chlorine; nitryl chloride

---

1. Introduction

Research over the past several decades has shown that the presence of reactive gas phase chlorine species, particularly chlorine radicals ($Cl^{\bullet}$), can contribute significantly to atmospheric reactivity [1–7]. High concentrations of $Cl^{\bullet}$ can lead to increased rates of Volatile Organic Compound (VOC) oxidation [8–13] and enhanced rates of O_3 production in the troposphere [1,3,7,14–16]. Photochemical sources of $Cl^{\bullet}$ include Cl_2 and HOCl [17], which are the primary forms of anthropogenic chlorine emissions [7,18,19]. Chlorine radicals, once produced, can participate in reactions with VOCs to produce alkyl radicals. These reactions typically proceed via hydrogen abstraction as shown in Reaction (R1), where R represents a generic VOC, and $R^{\bullet}$ represents the resulting alkyl radical [17,20].

$$Cl^{\bullet} + RH \rightarrow R^{\bullet} + HCl. \quad \text{(R1)}$$

Previous studies have reported field observations of elevated tropospheric Cl_2 at various locations across North America. Many of these observations were made near coastal areas, and maximum observed concentrations range from 20 ppt to 250 ppt [21–24]. Additionally, concentrations of up to 400 ppt Cl_2 were observed in the Arctic marine boundary layer in Barrow, Alaska [25]. Cl_2 source strengths on the order of 10–100 ppt $Cl_2 \cdot h^{-1}$ are required to explain such concentrations due to the rapid photolysis of Cl_2 [22,23,25].

Anthropogenic sources [1,26], aqueous reaction pathways [27,28] and naturally occurring heterogeneous or surface reaction routes of Cl_2 production [25,29,30] have been proposed to explain these observations. Previous experiments have observed that Cl_2 production from irradiated mixtures of O_3 and particulate chloride proceeds at a rate that is too rapid to be explained unless heterogeneous chemistry is active [30]. Numerous mechanisms have been proposed to explain the exact pathway for the heterogeneous formation of Cl_2. For example, the reaction of gas phase O_3 at the particle surface has been suggested [31,32].

$$2\ Cl^{-}_{(aq)} + O_{3(g)} \xrightarrow{H_2O} Cl_{2(g)} + 2\ OH^{-}_{(aq)} + O_{2(g)} \quad \text{(R2)}$$

Other work suggests that the reaction of hydroxyl radicals ($OH^{\bullet}$) at the particle surface more accurately depicts the chemistry active during heterogeneous Cl_2 production [30,33,34], where the formation of a surface complex between particulate Cl^{-} and gas phase $OH^{\bullet}$ was suggested as the rate limiting step, as is shown in Reactions (R3) and (R4).

$$OH_{(g)} + Cl^{-}_{(aq)} \rightarrow OH\bullet\bullet Cl^{-} \quad \text{(R3)}$$

$$2OH\bullet\bullet Cl^{-} \rightarrow Cl_{2(g)} + 2OH^{-}_{(aq)} \quad \text{(R4)}$$

Regardless of the exact mechanism, the presence of a heterogeneous route for significant Cl_2 production from particulate chloride has implications for air quality through the production of O_3 [16] and particulate matter.

Heterogeneous production of gas phase $ClNO_2$ from particulate chloride has also been shown to occur and can lead to the generation of $Cl^{\bullet}$ in the presence of sunlight [35–38]. $ClNO_2$ chemistry also decreases the loss of reactive nitrogen via N_2O_5 deposition by producing a photolytic form of reactive nitrogen that is reintroduced into the gas phase [39–42]. Heterogeneous routes for the production of Cl_2 from particulate chloride have also been shown to exist [30,42–44].

Observations [24,37,45–47], modeling work [39–42] and laboratory studies [36–38,48–52] in the recent past have identified heterogeneous $ClNO_2$ formation as a major route for the production of reactive gas phase chlorine. The mechanism of $ClNO_2$ production is initiated by the reactive uptake of N_2O_5 on chloride-containing aerosol particles, as seen in Reaction (R5). This reaction competes with the heterogeneous hydrolysis of N_2O_5 (Reaction (R6)), which produces HNO_3.

$$N_2O_{5(g)} + HCl_{(aq)} \rightarrow HNO_{3\,(g)} + ClNO_2 \quad \text{(R5)}$$

$$N_2O_{5(g)} + H_2O_{(l)} \rightarrow 2\ HNO_{3\,(aq)} \quad \text{(R6)}$$

This results in relatively unreactive particulate chloride being transformed into reactive gas phase chlorine. The $ClNO_2$ produced by the mechanism in Reaction (5) is photolytic and will decompose to produce gas phase NO_2 and $Cl^{\bullet}$ [17].

Aside from coastal [24,37,53,54] and oceanic [35] observations, several studies have recently reported significant $ClNO_2$ concentration in inland and mid-continental regions [45–47,55]. Previous measurements and modeling work have indicated that ppb-level concentrations of $ClNO_2$ are present in Houston, TX, USA and along the coast near the Houston Ship Channel [37,40,41]. The measurements reported here provide further insight into the formation and concentrations of Cl_2 and $ClNO_2$ at an inland location in southeast Texas and their implications to atmospheric reactivity.

2. Results and Discussion

The data presented in this work were collected during the DISCOVER-AQ 2013 campaign [56] in Houston, TX, USA for the period of 1 September 2013–1 October 2013. The data were obtained at an air quality monitoring ground site in Conroe, TX, USA (30.350278°N, 95.425000°W) situated next to the Lone Star Executive Airport in Montgomery county. The site is located approximately 60 km north northwest from the Houston urban center and approximately 125 km northwest of the nearest coastline. The gas phase species Cl_2, N_2O_5 and $ClNO_2$ were measured using an iodide High Resolution Time-of-Flight Chemical Ionization mass Spectrometer (HR-ToF-CIMS) and were identified by adduct ions Cl_2I^-, $N_2O_5I^-$, and $ClNO_2I^-$, respectively. The concentration and bulk composition of particulate matter smaller than 1 μm in diameter (PM_1) was measured using an Aerosol Chemical Speciation Monitor (ACSM, Aerodyne Research) [57]. Particle size distributions were measured using a Scanning Electrical Mobility System (SEMS, Brechtel Manufacturing).

Observations over the entire month of September 2013 revealed average peak concentrations of Cl_2, $ClNO_2$, and N_2O_5 of 1.6, 25, and 1.5 ppt, respectively. The highest concentrations of chlorine species were detected during the period of 11–20 September, and this time period is the focus of the following analysis. During this period, daily peak concentrations of Cl_2, $ClNO_2$, and N_2O_5 frequently exceeded 2 ppt, 60 ppt, and 20 ppt, respectively. Average nocturnal (8 p.m.–2 a.m.) concentrations of N_2O_5 were approximately 5 ppt. $ClNO_2$ morning (5 a.m.–11 a.m.) and nocturnal concentrations averaged 24 and 21 ppt, respectively. Cl_2 typically peaked in the afternoon, and Figure 1 shows the time series for 11–20 September.

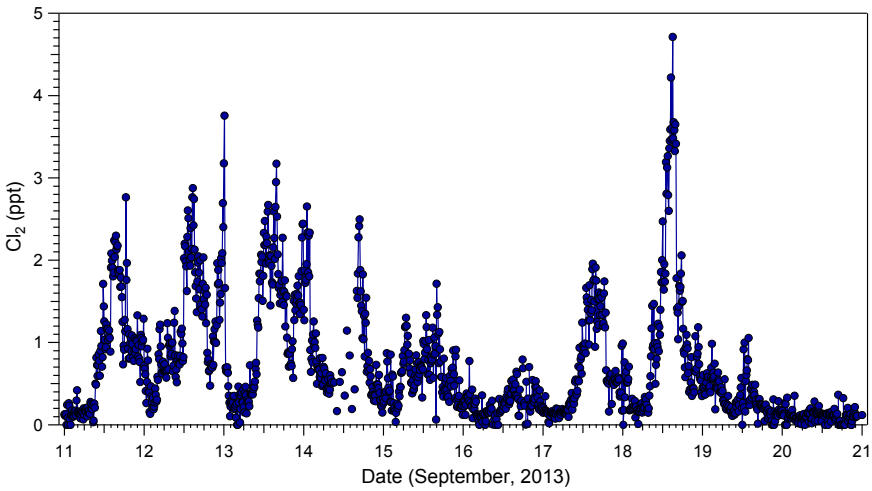

Figure 1. Time series of Cl_2 (10-min averages) at the Conroe, Texas measurement site from 11–21 September.

N_2O_5 exhibited peak nocturnal concentrations exceeding 20 ppt on the nights between 11–13 September. However, concentrations on most other nights rarely exceeded 2 ppt, even when increases in $ClNO_2$ concentrations were observed during the same time periods. Concentration time series of N_2O_5 and $ClNO_2$ from 11–21 September are shown in Figure 2. The implications of these observations are discussed further in the following sections.

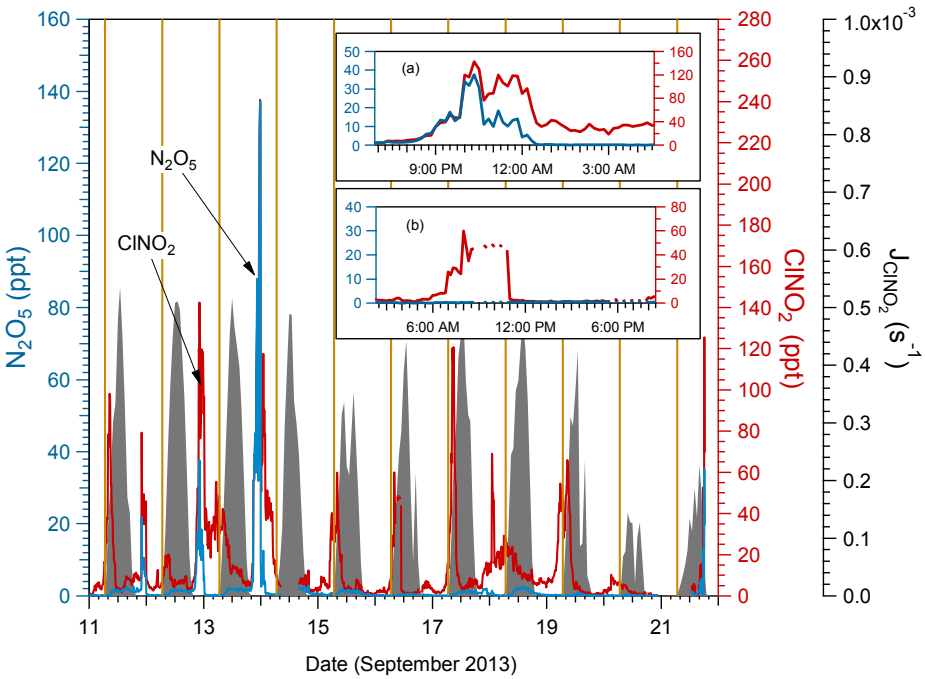

Figure 2. Time series of 10-min average $ClNO_2$ and N_2O_5 concentrations at the Conroe, Texas site from 11–21 September. Two distinct patterns were observed with respect to N_2O_5 and $ClNO_2$. Inset (**a**) shows a time period (9/13) when $ClNO_2$ and N_2O_5 concentrations correlated. Inset (**b**) shows a time period (9/16) when little N_2O_5 concentrations remained below the detection limit despite elevated $ClNO_2$ concentrations. A time series of the $ClNO_2$ photolysis rate is shown in grey, and vertical lines represent sunrise.

2.1. Cl_2 Measurements

Concentrations of Cl_2 typically peaked in the afternoon at concentrations ranging 1–10 ppt. During the afternoon hours (12:00–6:00 p.m.) on many days, Cl_2 concentrations remained above 1–2 ppt. On most days, Cl_2 peaked between 3:00 p.m. and 4:00 p.m. (Figure 1). Figure 3 shows the diurnal pattern of Cl_2 concentrations between 11–21 September.

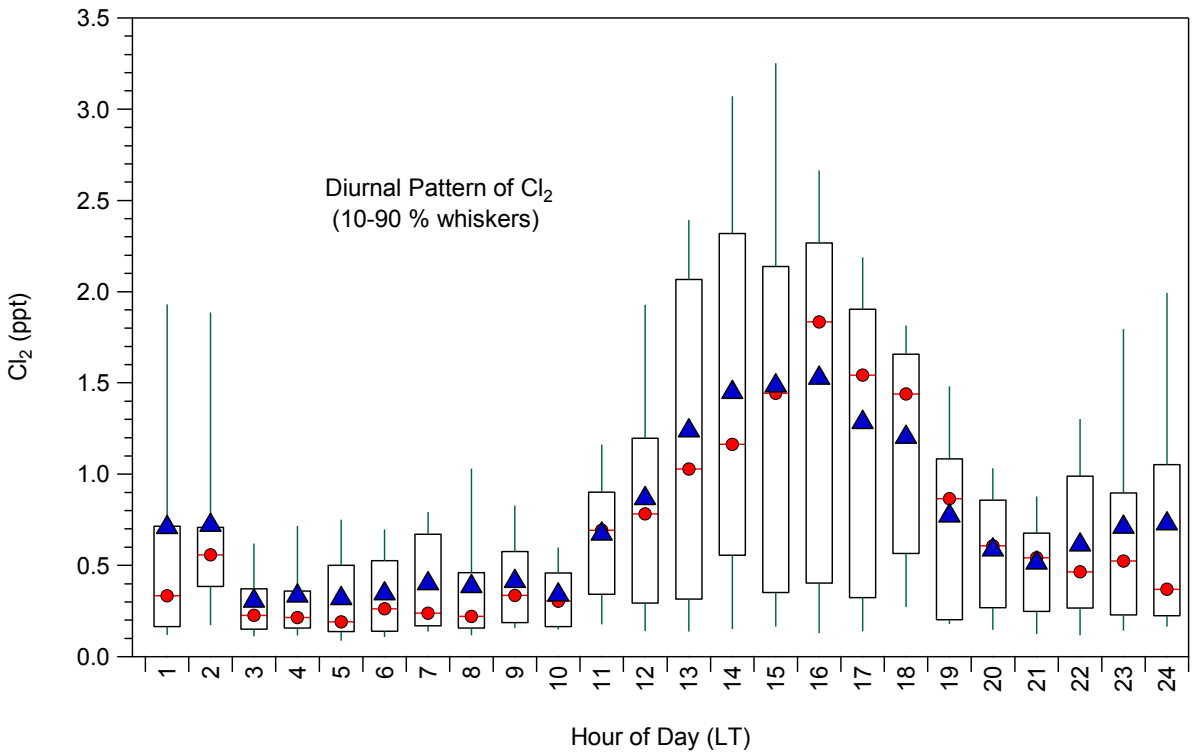

Figure 3. Diurnal pattern of Cl_2 concentrations observed from 11–21 September. Concentrations were typically elevated in the mid to late afternoon, with a lower enhancement late at night due to late night peaks such as the night of 12 and 13 September. Boxes indicate 25th and 75th percentiles, and whiskers indicate 10th and 90th percentiles.

These observed concentrations are slightly lower than concentrations observed in previous studies [22–24,58], and significantly lower than concentrations that have been detected in the arctic marine boundary layer [24,25]. However, the higher concentrations of Cl_2 in these previous studies would be expected since they were taken in coastal areas, in close proximity to a large sea salt source. Although the Cl_2 concentrations reported here are relatively low compared to other studies, the observation of a sustained concentration in spite of the rapid day-time photolysis of Cl_2 suggests a significant source of Cl_2 is present. For example, the average Cl_2 concentration between 2:00 p.m. and 2:30 p.m. on 18 September was 3.8 ppt. The calculated photolysis rate constant for this same period, using the coordinates of the measurement site, was 2.5×10^{-3} s^{-1}. This implies an approximate Cl_2 photolysis rate of 35 ppt $Cl_2 \cdot h^{-1}$ for a mid-day Cl_2 concentration of 4 ppt Cl_2; calculated 30-min average photolysis rates between 10:00 a.m. and 4:00 p.m. ranged from 7–35 ppt $Cl_2 \cdot h^{-1}$. Considering that concentrations on 18 September steadily increased from 10:00 a.m. and peaked at 2:00 p.m., this suggests that a minimum source strength of approximately 10–30 ppt$\cdot h^{-1}$ during the mid-day is necessary to explain the

observations. This is similar in strength to sources suggested by previous studies to explain Cl_2 observations elsewhere [22,23].

Similar daytime Cl_2 concentrations were observed for several other days during the campaign (Figure 1), suggesting that a similar source was present during those times as well. Such a Cl_2 source could potentially lead to the enhanced oxidation of CH_4 and other VOCs [23,25,58], and therefore enhanced formation of secondary organic aerosol. Additionally, enhanced O_3 production can result from the presence of a $Cl^{\bullet}$ source [1,33]. The implications of this are discussed further in Section 3.4.

On several occasions (13–15 September, for example), increases in Cl_2 were observed late at night or in the early morning, coinciding with increases in $ClNO_2$. No significant anthropogenic emissions of gas phase Cl_2 were known to be present in the area at the time. It is possible that the source of Cl_2 in these situations was the same as $ClNO_2$ since N_2O_5 has been shown to oxidize directly to Cl_2 when particles are acidic [43]. Recent measurements in inland regions suggest that soil deflation could possibly play a larger role as a particulate chloride source than previously assumed [59–61]. Considering the diurnal pattern of Cl_2, with peak concentrations occurring in the mid-afternoon, it is more likely that Cl_2 is produced inland. Gas phase Cl_2 transported from the coast would be degraded by photolysis by the time it reaches the measurement site, which could take several hours. Additionally, the heterogeneous production of reactive chlorine is thought to be driven by O_3 or $OH^{\bullet}$, species which peak during the mid-day. The timing of peak Cl_2 concentrations thus suggest a heterogeneous mechanism as a possible source of observed Cl_2.

2.2. $ClNO_2$ and N_2O_5 Measurements

For the month of September, 2013, $ClNO_2$ was frequently detected at concentrations exceeding 50 ppt (approximately 40% of the days in the month). Observations for the period spanning 11–21 September are shown in Figure 2. Although the timing of peak $ClNO_2$ concentration varied between days (e.g., Figure 2a compared to Figure 2b), the typical pattern was a peak $ClNO_2$ concentration between 25–60 ppt occurring between 7:00–10:00 a.m. Daily 1-hour maximum concentrations averaged 24 ppt over the course of the month. On several days, however, $ClNO_2$ concentrations peaked at night between 23:00–24:00, reaching concentrations over 100 ppt by midnight. Examples of such episodes can be seen in Figure 2 on the nights of 13 and 14 September. Observations of N_2O_5 were also made, and during periods when the concentration was high (11–13 September), N_2O_5 correlated well with $ClNO_2$. However, there were many days (e.g., 14–21 September) during which elevated concentrations of $ClNO_2$ were observed while N_2O_5 remained low or was below the detection limit, perhaps suggesting that $ClNO_2$ production was limited by N_2O_5 on these days.

Observed concentrations of $ClNO_2$ were lower than previous measurements made in coastal areas. During the Texas Air Quality Study II (TexAQS II), $ClNO_2$ concentrations reaching 1200 ppt were detected in the Houston Ship Channel [37]. At another coastal location, in Los Angeles, CA, concentrations up to 1500 ppt were detected off the California coast in the Los Angeles region [24]. The lower magnitude of $ClNO_2$ concentrations reported here is likely due to the fact that measurements were taken further inland (~125 km from the coast) and therefore further from a sea salt chloride source. However, the $ClNO_2$ concentrations observed in Conroe, TX, USA, are also lower than recent observations much further from the coast. For example, $ClNO_2$ concentrations of up to 800 ppt and 450 ppt were detected at Kohler Mesa, CO (~1400 km from coast) [46] and Hessen, Germany (~380 km from coast) [45],

respectively. The most likely explanation for these observations is that an inland source of chloride was present at these locations, and more recent work [59] suggest the presence of a significant soil source for chloride in Colorado. In this study, the measurements are consistent with the influence of a moderate particulate chloride source, and the observation that N_2O_5 was never present in the absence of $ClNO_2$ suggests that heterogeneous production was limited by N_2O_5 availability. The concentrations reported here are within the range predicted by previous modeling studies of $ClNO_2$ production in the region [39,40,42]. Concentrations of this magnitude were predicted to result in an enhancement of O_3 production up to several ppb [42].

On nights when $ClNO_2$ and N_2O_5 correlated well, the concentrations typically peaked around midnight (Figure 2a). However, when elevated $ClNO_2$ was present in the absence of N_2O_5, the concentrations typically peaked in the early to mid-morning (Figure 2b). Figure 4 shows a diurnal pattern of $ClNO_2$ and $PM_{2.5}$ surface area (as measured by the SEMS). Within the diurnal cycle of $ClNO_2$ at the measurement site, two distinct patterns of $ClNO_2$ concentrations are clearly visible. One pattern peaks early in the morning between 8 and 9 a.m., shortly after sunrise. In the other, late night $ClNO_2$ peaks are observed around midnight, coinciding with peak N_2O_5 concentrations (11–13 September). The peak 1-h average particulate surface area also occurs around the time of peak $ClNO_2$ concentrations in the early mornings, suggesting that conditions are favorable for the heterogeneous production of $ClNO_2$ from N_2O_5 in air masses that are advected to the site in the early mornings.

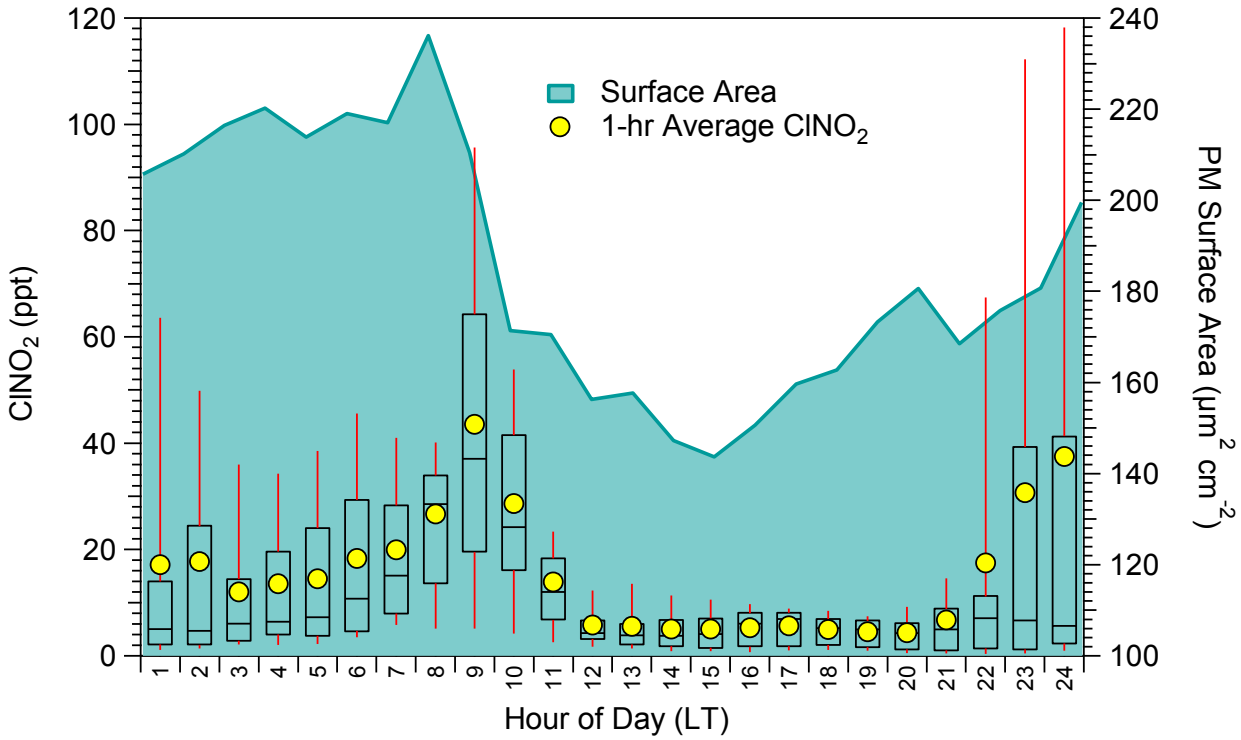

Figure 4. Diurnal cycle of $ClNO_2$ concentrations, showing two distinct patterns that are present during the campaign: (1) an early morning peak concentrations where $ClNO_2$ is advected to the site, and (2) late night peak concentrations, when $ClNO_2$ and N_2O_5 concentrations correlate significantly, suggesting more local inland production of $ClNO_2$.

Analysis of ACSM data collected during DISCOVER-AQ suggests high concentrations of particulate organic nitrates [62], which are formed either from photo-oxidation of hydrocarbons in the presence of NO_x or from the reactions of hydrocarbons with NO_3 radicals. Nitrate radical chemistry acts as a NO_y sink, reducing the formation of N_2O_5 and therefore $ClNO_2$ and could be responsible for relatively low N_2O_5 concentrations observed throughout most of the campaign.

2.3. Air Source Regions and Back Trajectories

On several days during the campaign, differences in the correlation of $ClNO_2$ and N_2O_5 concentrations and the timing of $ClNO_2$ peak concentrations suggest possible differences in the production and transport of $ClNO_2$. To investigate this difference further, HYSPLIT back trajectories were calculated for each case [63]. Starting height was set to 70 m, the end point of the back trajectories was set to the coordinates of the Conroe field site, and the end time was set to the time of maximum observed $ClNO_2$ concentration on each night. The model was used to generate a new back trajectory every two hours from the start time for a total of six 24-h back trajectories for each time period. Figure 5 shows a comparison of calculated back trajectories for the 13th and 16th of September.

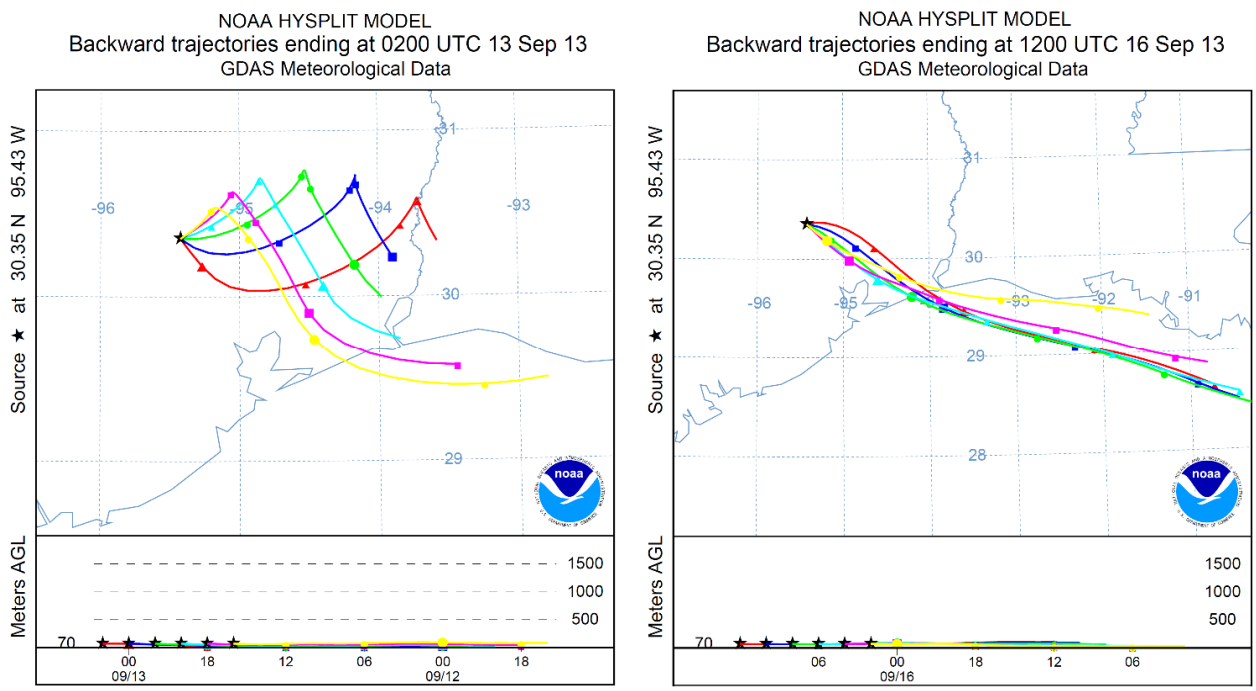

Figure 5. A comparison of HYSPLIT back trajectories for the days shown in the insets of Figure 2. Left: Back trajectories for the morning of 13 September 2013. The back trajectories ending at the time of peak $ClNO_2$ concentrations (10–11 p.m.) show air that originated inland near the TX-LA border 24 hours prior. Right: Back trajectories for the morning of 16 September 2013. The back trajectory at the time of peak $ClNO_2$ concentration (7–8 a.m.) indicates that the air mass originated in the Gulf of Mexico 24 hours prior, passing between the Houston, TX region and the LA-TX border.

One major difference between the two back trajectories is the amount of time that the air mass spent over land or over sea prior to arriving at the site. For example, air that was sampled at the site on

15–16 September originated in the Gulf of Mexico, resulting in a lower residence time over industrialized regions relative to the air sampled on the night of 12–13 September. Observations on the night of the 15th of September indicated very low N_2O_5. Elevated morning-time concentrations of $ClNO_2$ in these scenarios (e.g., 15–17 September) most likely resulted from transport of $ClNO_2$ to the measurement site from the Gulf Coast. $ClNO_2$ concentrations of up to 1.2 ppb were previously detected along the coast [37] where HYSPLIT back trajectories indicate the air originated on 16 September (Figure 5). The lack of a corresponding increase in N_2O_5 concentrations during these early morning episodes also suggests that the $ClNO_2$ observed at these times is produced elsewhere. The total amount of $ClNO_2$ transported to the site on these mornings was probably limited by N_2O_5 availability since SEMS data indicate that the highest measured particulate surface area concentrations were observed during these times (Figure 4).

In contrast to the early morning peak concentrations, the air that was sampled on the night of 12 September originated inland, and the majority of its path was over land. On the night of 12 September, it might be expected that the observed air mass had been exposed to additional inland NO_x sources that would explain the higher N_2O_5 concentration relative to the night of 15–16 September.

On several occasions, $ClNO_2$ was found to be elevated in the afternoon during daylight hours. Examples of this include the afternoons of 12, 13 and 17 September. Back trajectories for the afternoon hours on these days indicate that air transported to the site originated along the Gulf coast. On the afternoon of 12 September between the hours of 1 and 5 p.m., incoming air originated along the gulf coast 18 hours prior to arriving at the site. The back trajectories for 13 and 17 September indicate that the air masses originated from the same region, frequently crossing the region between Lake Charles, LA and Houston, TX. The amount of $ClNO_2$ that would need to be produced in the transported air can be estimated. For example, $ClNO_2$ concentrations on the afternoons of 12 and 13 September were approximately 10–15 ppt. An air mass arriving at 2 p.m. would have been exposed to daylight for approximately 7 hours. Taking the average observed photolysis rate of $ClNO_2$ between 7 a.m. and 2 p.m. for these dates, this corresponds to an average $ClNO_2$ photolysis rate of 2.8×10^{-4} s^{-1}. This suggests that approximately 1–2 ppb of $ClNO_2$ would need to be produced in the incoming air masses during transport to the site in order for concentrations on the order of 10 ppt to be observed. Previous measurements and modeling predictions in this region indicate that elevated concentrations of $ClNO_2$ can reach concentrations of this magnitude [37,39,40,42].

Back trajectories in the afternoons when Cl_2 concentrations were typically elevated indicate that air is transported directly from the Gulf of Mexico, often passing over the metropolitan area of Houston, TX, USA. For example, air sampled at the site between 12–5 p.m. on the afternoon of 12, 13, 16 and 18 September consistently originated from the Gulf of Mexico 12 to 18 hours before being sampled. The transport of these air masses from the coast could suggest that long range sea salt transport contributed as a source of heterogeneously produced Cl_2 at the site.

2.4. Box Modeling Results

The contribution of observed Cl_2 and $ClNO_2$ to $Cl^{\bullet}$ production and resulting atmospheric reactivity were analyzed using ambient box modeling. The Statewide Air Pollution Research Center (SAPRC) software was used in combination with an updated version of the Carbon Bond 6 (CB6r2) chemical

kinetics mechanism [64,65]. The CB6r2 mechanism was modified to include basic gas phase chlorine chemistry [65,66] in addition to Cl_2 and $ClNO_2$ photolysis in a manner similar to Sarwar *et al.* [39]. A list of reactions that were added is provided in the supplementary material. The photolysis rate of Cl_2 was calculated internally to the mechanism for a latitude and longitude matching the location of the measurement site. For the dates used in the simulations, this resulted in a peak j_{Cl_2} of 2.8×10^{-2} s^{-1}, occurring at 12:30 p.m. Deposition was not included and boundary layer height was fixed for the duration of the model run.

Conditions on 18 September were modeled in order to assess the effects of Cl_2 on atmospheric reactivity. Although this day did not have the highest concentration of Cl_2 observed throughout the campaign (Figure 1), sustained concentrations over 2 ppt were observed for the entire period between 12:00–6 p.m., suggesting a continuous source of Cl_2 was present. Emissions of Cl_2 were added to the model so that the observed Cl_2 concentration profile was replicated in the simulations. On this day, relative humidity was 98% at 6:00 a.m., dropping to a minimum of 43% by 2:00 p.m., and temperature rose from 294 K at 6:00 am to 308 K at 2:00 p.m. Initial concentrations included 0.4 ppt Cl_2, 8 ppb NO_2, and 10 ppb O_3, consistent with early morning observations at the site on 18 September. Using these initial conditions and meteorological inputs, the production of OH radicals was calculated Equation (1), and day-time OH production ranged 10^6–10^7 molecules·cm^{-3} s^{-1}. A typical urban VOC mixture [67] was included in simulations at a concentration of 20 ppbC. Four scenarios were simulated: (1) no Cl_2 and no VOCs, (2) including Cl_2 emissions, no VOCs, (3) no Cl_2 emissions with 20 ppbC VOCs and (4) including Cl_2 emissions and 20ppbC VOCs. $Cl^{\bullet}$ production was calculated from the photolysis of measured Cl_2 concentrations Equation (2); an average emissions rate of 15 ppt·h^{-1} between 8:00 a.m.–6:00 p.m. was found to be necessary to replicate the observed concentrations. A comparison of modeled $OH^{\bullet}$ and $Cl^{\bullet}$ production rates and concentrations are shown in Figure 6.

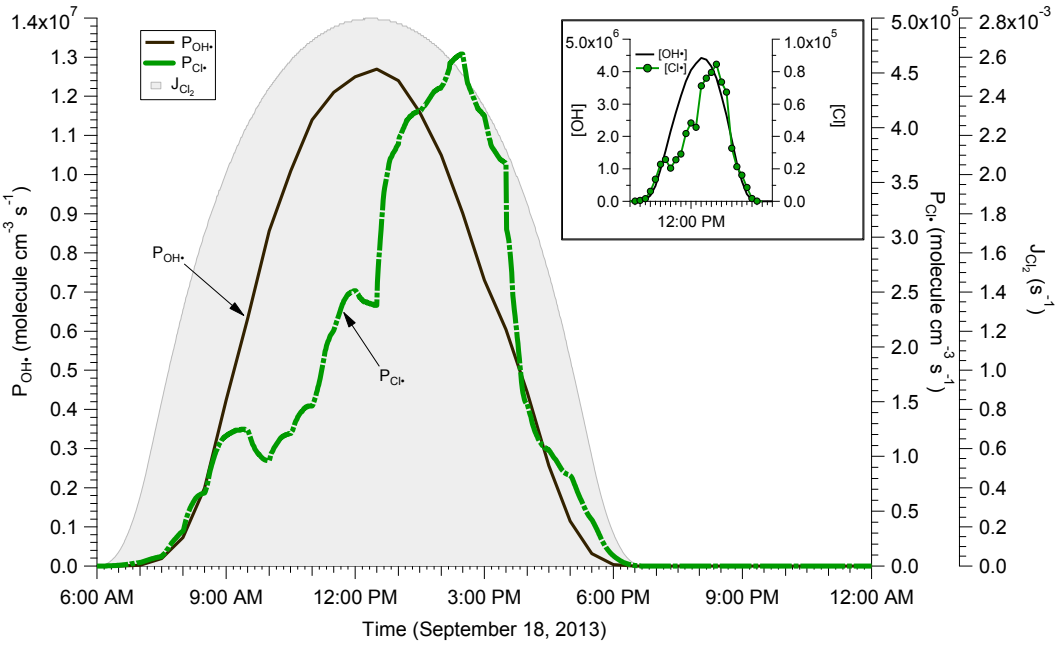

Figure 6. Production of OH and Cl radicals in a box modeling simulations for the conditions on 18 September 2013. The inset shows calculated concentrations of OH and Cl radicals in molecules·cm^{-3}·s^{-1}.

Although $Cl^{\bullet}$ production rates and concentrations are approximately 1–2 orders of magnitude lower than those of $OH^{\bullet}$, the calculated concentrations are significant when the relative reactivity of the two radicals is taken into account. The rate constants for the reactions of $Cl^{\bullet}$ with many VOCs is significantly (up to 100 times) faster than the corresponding reactions of $OH^{\bullet}$ [9–11,68,69]. Thus, $Cl^{\bullet}$ concentrations on the order of 10^5 molecules·cm^{-3} s^{-1} represent a significant radical source with respect to the oxidation of VOCs. For example, taking the maximum $Cl^{\bullet}$ concentration (8.5×10^4 molecules·cm^{-3}) and the corresponding $OH^{\bullet}$ concentration at the same time (3.6×10^6 molecules·cm^{-3}), the rate constant for the reaction of $Cl^{\bullet}$ and $OH^{\bullet}$ with CH_4 at 298 K are approximately 1.0×10^{-13} and 6.4×10^{-15} cm^3 molecules^{-1} s^{-1}, respectively. Assuming a CH_4 concentration of 1700 ppb, this corresponds to rates of reaction with CH_4 for $Cl^{\bullet}$ and $OH^{\bullet}$ of 3×10^5 and 8×10^5 molecules·cm^{-3} s^{-1}, respectively. These rates of reaction indicate that the $Cl^{\bullet}$ from observed concentrations of Cl_2 could significantly contribute to atmospheric reactivity with respect to VOC oxidation. It is also important that Cl_2 and $Cl^{\bullet}$ peak in the mid to late afternoon when $OH^{\bullet}$ production begins to wane.

Measured O_3 concentrations on the morning of 18 September were low with concentrations reaching around 5 ppb at 6:00 a.m. Simulations under-predicted day-time O_3 concentrations by over 25% compared to measurements. Transport of O_3 to the site in the afternoon (which is not included in this box modeling simulation) likely leads to higher observed O_3 concentrations. O_3 production was found to be enhanced by Cl_2. The addition of Cl_2 without VOC (model scenario 1 *vs.* 2) increased maximum modeled O_3 concentration between 8:00 a.m.–6:00 p.m. by 10% (1 ppb) and $RO_2^{\bullet}$ concentration by up to 50% (1.1 ppt). The addition of Cl_2 in the presence of VOC (model scenario *3 vs.* 4) increased the maximum day-time O_3 concentration by 8% (2 ppb) and $RO_2^{\bullet}$ concentration by 28% (10 ppt). These results are summarized in Table 1.

Conditions on the morning of 13 September (scenario 5 and 6) and 16 September (scenarios 7 and 8) were modeled in order to assess the effects of $ClNO_2$ on atmospheric reactivity. Relative humidity and temperature in the model were set to approximate conditions present at the Conroe site. The simulation start time was set to midnight in order to capture the changes in radical production between nocturnal and early morning conditions. Model inputs for 13 September also included initial concentrations of 35 ppb O_3 and 20 ppb NO_x (consistent with measurements), as well as 20 ppbC VOC. A base case model run was performed without $ClNO_2$ (scenario 5) and compared to the model run with 40 ppt initial $ClNO_2$ (scenario 6). Model inputs for 16 September included initial concentrations of 15 ppb O_3 and 10 ppb NO_x (consistent with measurements), as well as 20 ppbC VOC. A base case with no $ClNO_2$ (scenario 7) was compared to a separate model run (scenario 8), where initial $ClNO_2$ concentrations were set to 0, and $ClNO_2$ emissions were added to gradually increase the total amount of $ClNO_2$ from 0 to 50 ppt between 6–8 a.m. (Figure 2b).

A comparison of the radical production rates of $OH^{\bullet}$ and $Cl^{\bullet}$ resulting from measured $ClNO_2$, O_3 and H_2O concentrations is shown in Figure 7. Although $Cl^{\bullet}$ production reaches a peak rate that is approximately 2 orders of magnitude lower than peak $OH^{\bullet}$ production, its production in the early morning increases atmospheric reactivity during a time when $OH^{\bullet}$ concentrations are low. Concentrations of $Cl^{\bullet}$ peak in the very early morning (Figure 7 inset), approximately two hours before $OH^{\bullet}$ concentrations begin to increase. Using the peak modeled $Cl^{\bullet}$ concentration (2.5×10^4 molecules·cm^{-3} and an approximate $OH^{\bullet}$ concentration from the same time period (1.5×10^6 molecules·cm^{-3}), the reaction rates with 1700 ppb CH_4 are similar at 1.1×10^5 and 4.1×10^5 molecules·cm^{-3} s^{-1} for $Cl^{\bullet}$ and $OH^{\bullet}$, respectively.

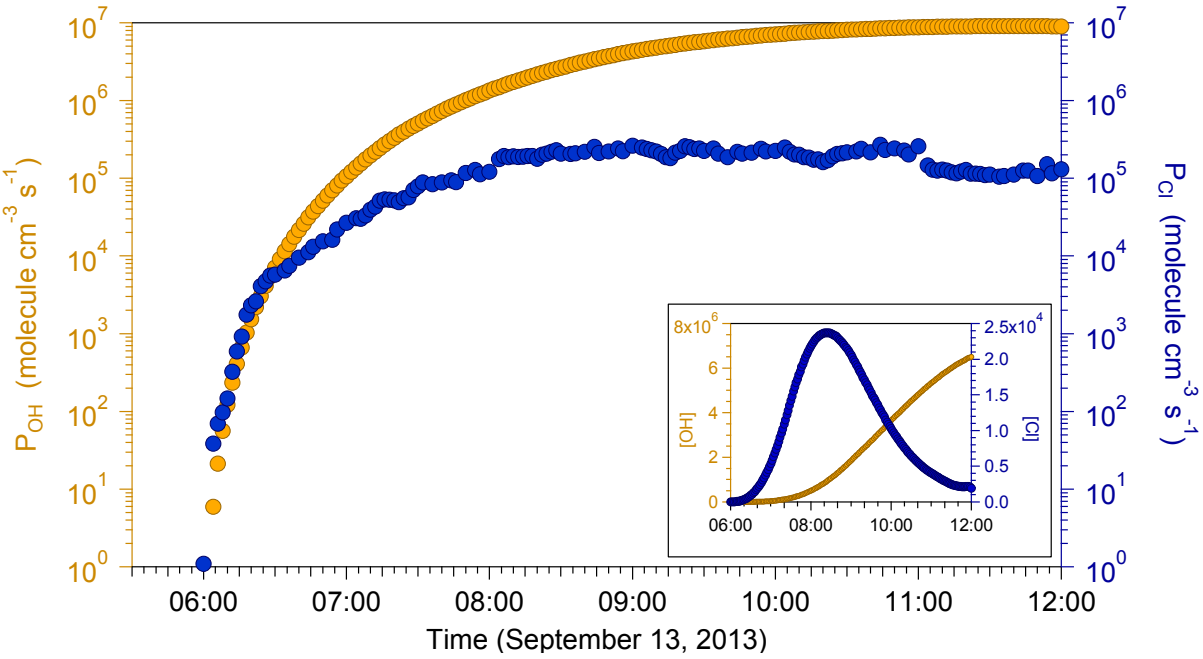

Figure 7. OH• production resulting from the photolysis of O_3 compared to Cl• production from observed concentrations of $ClNO_2$ on the morning of 13 September 2013. The inset shows a comparison of modeled Cl• and OH• radical concentrations (molecules·cm^{-3}) during the same time period, assuming an initial $ClNO_2$ concentration of 40 ppt (model scenario 6).

The inclusion of 40 ppt $ClNO_2$ enhanced O_3 and RO_2• concentrations between 7:00 a.m.–3:00 p.m. by a maximum of 6.5% and 0.4%, respectively, when compared to a simulation with no $ClNO_2$ (scenarios 5 and 6 in Table 1). For simulations on the morning of 16 September, which included emissions of 50 ppt $ClNO_2$ in the early morning, similar enhancements in O_3 and RO_2• concentrations were observed: in the presence of 20 ppbC VOC, O_3 and RO_2 concentrations were enhanced by 11.5% and 1.0%, respectively, when compared to a base case simulation without $ClNO_2$ (scenarios 7 and 8 in Table 1). In the absence of VOCs the addition of $ClNO_2$ did not significantly increase O_3 or RO_2• concentrations (not listed in Table 1). The increases in RO_2• exemplify how $ClNO_2$ at the observed concentrations can contribute significantly to atmospheric reactivity, particularly in the morning. A summary of these modeling results and the results of Cl_2 simulations are listed in Table 1.

Table 1. Summary of Modeling Results.

Scenario	Chlorine Species	Comparison	[VOC] (ppbC)	$\Delta[O_3]_{max}$ (%)	$\Delta[RO_2^{\bullet}]_{max}$ (%)
1	--	1	0	10	50
2	Cl_2		0		
3	--	2	20	8	28
4	Cl_2		20		
5	--	3	20	6	0.4
6	$ClNO_2$		20		
7	--	4	20	12	1
8	$ClNO_2$		20		

3. Experimental Section

The area surrounding the air-quality monitoring station at Conroe, TX is primarily affected by pollution in the outflow of air from Houston, which hosts significant energy and petrochemical industries in addition to a large urban population. The regional atmospheric chemistry is also influenced by marine air from the Gulf of Mexico. The site itself is located in the middle of a field adjacent to the airport, with a gravel parking lot nearby and bordered by trees approximately 200 m to the North.

A permanent Texas Commission on Environmental Quality (TCEQ) ambient measurement station exists at this site and provided continuous meteorological data (wind speed, wind direction, temperature and relative humidity) for the duration of the campaign. NO_x and O_3 monitors were also present at the TCEQ site. During DISCOVER-AQ a temporary ground site was set up adjacent to the permanent station. Chlorine species were detected using a High Resolution Time-of-Flight Chemical Ionization Mass Spectrometer (HR-ToF-CIMS, henceforth referred to as CIMS) [70–73], which was operated in negative ionization mode utilizing the iodide reagent ion. Similar CIMS techniques have been used in previous studies for the detection of $ClNO_2$, N_2O_5 and Cl_2 [24,35,37,45–47,74,75], and other studies have described in detail the operation and application of the Aerodyne CIMS. Species reported here that were detected with the iodide CIMS included $ClNO_2$, Cl_2 and N_2O_5; the ions monitored for these species were $IClNO_2^-$, ICl_2^-, and $IN_2O_5^-$.

A sample flow of 2 LPM was introduced into the instrument through a ¼" outer diameter perfluoroalkoxy (PFA) Teflon® sample line connected to the stainless steel inlet by a ¼" to 10 mm stainless steel Swagelok union. The sample flow then passed into the ion-molecule reaction (IMR) chamber of the instrument, where it was mixed with a reagent ion flow of 2 LPM. Ionization in the IMR took place at a pressure of 200 mbar and temperature of 34°C (controlled by an IMR heater). $I(H_2O)_n^-$ reagent ions were generated by passing a flow of ultra-high purity (UHP) N_2 over a methyl iodide (CH_3I, Sigma Aldrich, 99%) permeation tube. The N_2 flow first passed through purified water (Milli-Q, model Advantage-A10) upstream of the CH_3I permeation tube in order to provide the humidity necessary for sufficient production of H_2OI^- ions. This also helped to stabilize the relative humidity within the IMR and resulting variations in sensitivity that have been noted for iodide chemical ionization [35,72]. Inside of the inlet, the sample flow then passed through 44.5 mm of the 10 mm outer diameter stainless steel tubing before passing through a critical orifice into the IMR. After mixing in the IMR the combined reagent and sample flow passed through two quadrupoles before entering the Time-of-Flight (ToF) mass analyzer. During the entire measurement period, the ToF was operated in V mode, providing higher sensitivity but lower resolution than W mode.

In order to test for measurement artifacts a flow of ultra-high purity (UHP) N_2 was periodically introduced into the sampling inlet. This flushing of the sampling line resulted in a rapid drop to background levels in the signals for Cl_2, N_2O_5 and $ClNO_2$, suggesting that adsorption and subsequent desorption of these species from the inlet line walls was not a significant source of measurement artifacts. When the sampling commenced afterwards ion signals returned rapidly to ambient levels, suggestive of a high transmission efficiency. No explicit tests were performed to assess the N_2O_5 transmission efficiency in the field introducing uncertainty in the quantification of N_2O_5 which could be lost irreversibly to the inlet walls. The N_2O_5 concentrations in this study are reported assuming that transmission efficiency was equivalent to that observed during calibrations. We estimate that this

introduces a measurement uncertainty of 20%, a conservative estimate compared to previous work [76] which cited a ± 7% accuracy for N_2O_5 measured using a different instrument.

Equations (1) and (2) were used to calculate the production of $Cl^{\bullet}$ and $OH^{\bullet}$ consistent with box modeling simulation results. The production of $OH^{\bullet}$ was calculated from the reactions of $O(^1D)$ with H_2O, N_2, and O_2 (Equation (1)), in a manner similar to a previous observational study [45]. The rate of O_3 photolysis was used to calculate the rate of $O(^1D)$ generation, and additional details on the derivation of Equation (1) are described in the supplementary material. The production of $Cl^{\bullet}$ proceeded directly from the photolysis of Cl_2 (Equation (2)).

$$P_{OH} = 2J_{(O_3)}[O_3]k_{H_2O}[H_2O]/(k_{H2O}[H_2O] + k_{N2}[N_2] + k_{O2}[O_2]) \quad (1)$$

$$P_{Cl} = 2 \times j_{Cl_2}[Cl_2] \quad (2)$$

Additional simulations were performed to assess the impact of observed $ClNO_2$ concentrations on $Cl^{\bullet}$ production and atmospheric reactivity, and Equation (3) was used to quantify the production of $Cl^{\bullet}$ from $ClNO_2$.

$$P_{Cl} = j_{ClNO2}[ClNO_2] \quad (3)$$

4. Conclusions

During the month of September 2013, concentrations of Cl_2 and $ClNO_2$ regularly reached or exceeded 2 ppt and 60 ppt, respectively, at an inland monitoring site in Southeast Texas. The concurrent presence or absence of N_2O_5 at the site depended on the source of the sampled air, and longer paths over land corresponded to higher concentrations of N_2O_5. Peak $ClNO_2$ concentrations in the early mornings when little to no N_2O_5 was present on some days suggest that the production and transport of $ClNO_2$ from a non-local source is occurring. Contemporaneous measurements of PM surface area suggest conditions favorable to heterogeneous conversion of N_2O_5 in the advected air masses on these mornings. The presence of Cl_2 and $ClNO_2$ at the site are significant due to their role as $Cl^{\bullet}$ sources. Although Cl_2 concentrations are lower in magnitude, the fact that Cl_2 concentrations consistently peak in the afternoon when photolysis rates are highest suggests a Cl_2 source of approximately 30 ppt·h^{-1} Cl_2. Box modeling simulations suggest that such concentrations can contribute to enhanced O_3 and $RO_2^{\bullet}$ production during the day. The source of $ClNO_2$ is likely the result of reactions between anthropogenic NO_x sources and particulate chloride originating along the Gulf Coast, and the reported values are within the range of previous model predictions in the region. Assuming that the surface measurements made in the early morning are representative of the entire nocturnal boundary layer, $ClNO_2$ was also found to contribute to $Cl^{\bullet}$ production and atmospheric reactivity, particularly in the early morning before significant $OH^{\bullet}$ production begins. Overall, the results suggest that Cl_2 and $ClNO_2$ affect atmospheric reactivity and can impact the formation of ozone and secondary organic aerosol. In a region where attainment of the National Ambient Air Quality Standard for ozone has been an issue in the past decades, quantifying the effects of reactive chlorine chemistry is important for assuring future attainment.

Acknowledgments

This work was funded in part through a grant from the Texas Commission on Environmental Quality (TCEQ), administered by The University of Texas through the Air Quality Research Program (Project 12-012). The contents, findings opinions and conclusions are the work of the authors and do not necessarily represent findings, opinions or conclusions of the TCEQ. The work was also funded in part with funds from the State of Texas as part of the program of the Texas Air Research Center. The contents do not necessarily reflect the views and policies of the sponsor nor does the mention of trade names or commercial products constitute endorsement or recommendation for use. The authors would like to acknowledge the support of the entire DISCOVER-AQ Texas 2013 team. Code for the SAPRC box modeling software can be found at http://www.engr.ucr.edu/~carter/SAPRC. Meteorological data used for model input can be obtained via the TCEQ website (http://www.tceq.state.tx.us).

Author Contributions

Cameron Faxon, Jeffrey Bean, and Lea Hildebrandt Ruiz planned, prepared and conducted the ambient measurements. Cameron Faxon conducted the box model simulations and analyzed ambient data and box model results presented in this work. The manuscript was written by Cameron Faxon with the guidance of Lea Hildebrandt Ruiz.

Conflicts of Interest

The authors declare no conflict of interest.

References

1. Tanaka, P.L.; Riemer, D.D.; Chang, S.; Yarwood, G.; McDonald-Buller, E.C.; Apel, E.C.; Orlando, J.J.; Silva, P.J.; Jimenez, J.L.; Canagaratna, M.R.; *et al.* Direct evidence for chlorine-enhanced urban ozone formation in Houston, Texas. *Atmos. Environ.* **2003**, *37*, 1393–1400.
2. Wang, L.; Thompson, T.; McDonald-Buller, E.C.; Allen, D.T. Photochemical modeling of emissions trading of highly reactive volatile organic compounds in Houston, Texas. 2. Incorporation of chlorine emissions. *Environ. Sci. Technol.* **2007**, *41*, 2103–2107.
3. Faxon, C.B.; Allen, D.T. Chlorine chemistry in urban atmospheres: A review. *Environ. Chem.* **2013**, *10*, 221–233.
4. Wingenter, O.W.; Sive, B.C.; Blake, N.J.; Blake, D.R.; Rowland, F.S. Atomic chlorine concentrations derived from ethane and hydroxyl measurements over the equatorial Pacific Ocean: Implication for dimethyl sulfide and bromine monoxide. *J. Geophys. Res.* **2005**, *110*, doi:10.1029/2005JD005875.
5. Graedel, T.E.; Keene, W.C. Tropospheric budget of reactive chlorine. *Glob. Biogeochem. Cycles* **1995**, *9*, 47–77.
6. Keene, C.; Aslam, M.; Khalil, K.; Erickson, J.; Archie, I.I.I.; Graedel, E.; Loberr, M.; Aucott, M.L.; Ling, S.; Harper, D.B.; *et al.* Composite global emissions of reactive chlorine from anthropogenic and natural sources : Reactive chlorine emissions inventory. *J. Geophys. Res.* **1999**, *104*, 8429–8440.

7. Sarwar, G.; Bhave, P.V. Modeling the effect of chlorine emissions on ozone levels over the eastern United States. *J. Appl. Meteorol. Climatol.* **2007**, *46*, 1009–1019.
8. Liu, C.L.; Smith, J.D.; Che, D.L.; Ahmed, M.; Leone, S.R.; Wilson, K.R. The direct observation of secondary radical chain chemistry in the heterogeneous reaction of chlorine atoms with submicron squalane droplets. *Phys. Chem. Chem. Phys.* **2011**, *13*, 8993–9007.
9. Wang, L.; Arey, J.; Atkinson, R. Reactions of chlorine atoms with a series of aromatic hydrocarbons. *Environ. Sci. Technol.* **2005**, *39*, 5302–10.
10. Nelson, L.; Rattigan, O.; Neavyn, R.; Sidebottom, H. Absolute and relative rate constants for reactions of hydroxyl radicals and chlorine atoms with series of aliphatic alcohols and ethers at 298K. *Int. J. Chem. Kinet.* **1990**, *22*, 1111–1126.
11. Aschmann, S.M.; Atkinson, R. Rate Constants for the Gas-Phase Reactions of alkanes with Cl atoms at 296. *Int. J. Chem. Kinet.* **1995**, *27*, 613–622.
12. Canosa-Mas, C.E.; Hutton-Squire, H.R.; King, M.D.; Stewart, D.J.; Thompson, K.C.; Wayne, R.P. Laboratory Kinetic Studies of the Reactions of Cl Atoms with Species of Biogenic Origin: Δ3-Carene, Methacrolein and Methyl Vinyl Ketone. *J. Atmos. Chem.* **1999**, *34*, 163–170.
13. Ragains, M.L.; Finlayson-Pitts, B.J. Kinetics and mechanism of the reaction of Cl atoms with 2-Methyl-1,3-butadiene (Isoprene) at 298 K. *J. Phys. Chem. A* **1997**, *5639*, 1509–1517.
14. Chang, S.; McDonald-Buller, E.; Kimura, Y.; Yarwood, G.; Neece, J.; Russell, M.; Tanaka, P.; Allen, D. Sensitivity of urban ozone formation to chlorine emission estimates. *Atmos. Environ.* **2002**, *36*, 4991–5003.
15. Tanaka, P.L.; Allen, D.T.; Mullins, C.B. An environmental chamber investigation of chlorine-enhanced ozone formation in Houston, Texas. *J. Geophys. Res.* **2003**, *108*, doi:10.1029/2002JD003314.
16. Knipping, E.M.; Dabdub, D. Impact of chlorine emissions from sea-salt aerosol on coastal urban ozone. *Environ. Sci. Technol.* **2003**, *37*, 275–284.
17. Sander, S.P.; Friedl, R.R.; Barker, J.R.; Golden, D.M.; Kurylo, M.J.; Sciences, G.E.; Wine, P.H.; Abbatt, J.P.D.; Burkholder, J.B.; Kolb, C.E.; *et al.* Chemical Kinetics and Photochemical Data for Use in Atmospheric Studies: Evaluation Number 17. Available online: https://jpldataeval.jpl.nasa.gov/pdf/JPL%2010-6%20Final%2015Jun8011.pdf (accessed on 31 August 2015).
18. Chang, S.; Allen, D.T. Chlorine chemistry in urban atmospheres: Aerosol formation associated with anthropogenic chlorine emissions in southeast Texas. *Atmos. Environ.* **2006**, *40*, 512–523.
19. Chang, S.; Tanaka, P.; Mcdonald-buller, E.; Allen, D.T. Emission inventory for atomic chlorine precursors in Southeast Texas. Available online: http://www.tceq.state.tx.us/assets/public/implementation/air/am/contracts/reports/oth/EmissioninventoryForAtomicChlorinePrecursors.pdf (accessed on 31 August 2015).
20. Atkinson, R.; Baulch, D.L.; Cox, R.A.; Crowley, J.N.; Hampson, R.F.; Hynes, R.G.; Jenkin, M.E.; Rossi, M.J.; Troe, J. Evaluated kinetic and photochemical data for atmospheric chemistry: Volume III—Gas phase reactions of inorganic halogens. *Atmos. Chem. Phys.* **2007**, *7*, 981–1191.
21. Pszenny, A.A.P.; Keene, W.C.; Jacob, D.J.; Fan, S.; Maben, J.R.; Zetwo, M.P. Evidence of inorganic chlorine gases other than hydrogen chloride in marine surface air. *Geopys. Res. Lett.* **1993**, *20*, 699–702.

22. Spicer, C.; Chapman, E.; Finlayson-Pitts, B.; Plastrige, R.; Hubbe, J.; Fast, J.; Berkowitz, C. Unexpectedly high concentrations of molecular chlorine in coastal air. *Nature* **1998**, *394*, 353–356.
23. Finley, B.D.; Saltzman, E.S. Measurement of Cl_2 in coastal urban air. *Geophys. Res. Lett.* **2006**, *33*, doi:10.1029/2006GL025799.
24. Riedel, T.P.; Bertram, T.H.; Crisp, T.A.; Williams, E.J.; Lerner, B.M.; Vlasenko, A.; Li, S.M.; Gilman, J.; de Gouw, J.; Bon, D.M.; *et al.* A Nitryl chloride and molecular chlorine in the coastal marine boundary layer. *Environ. Sci. Technol.* **2012**, *46*, 10463–10470.
25. Liao, J.; Huey, L.G.; Liu, Z.; Tanner, D.J.; Cantrell, C.A.; Orlando, J.J.; Flocke, F.M.; Shepson, P.B.; Weinheimer, A.J.; Hall, S.R.; *et al.* High levels of molecular chlorine in the Arctic atmosphere. *Nat. Geosci.* **2014**, *7*, 91–94.
26. Chang, S.; Allen, D.T. Atmospheric chlorine chemistry in southeast Texas: impacts on ozone formation and control. *Environ. Sci. Technol.* **2006**, *40*, 251–262.
27. Oum, K.W.; Lakin, M.J.; DeHaan, D.O.; Brauers, T.; Finlayson-Pitts, B.J. Formation of molecular chlorine from the photolysis of ozone and aqueous sea-salt particles. *Science* **1998**, *279*, 74–76.
28. Herrmann, H.; Majdik, Z.; Ervens, B.; Weise, D. Halogen production from aqueous tropospheric particles. *Chemosphere* **2003**, *52*, 485–502.
29. Sadanaga, Y.; Hirokawa, J.; Akimoto, H. Formation of molecular chlorine in dark condition: Heterogeneous reaction of ozone with sea salt in the presence of ferric ion. *Geophys. Res. Lett.* **2001**, *28*, 4433–4436.
30. Knipping, E.M. Experiments and simulations of ion-enhanced interfacial chemistry on aqueous NaCl aerosols. *Science* **2000**, *288*, 301–306.
31. Behnke, W.; Zetzsch, C. Heterogeneous formation of chlorine atoms from various aerosols in the presence of O_3 and HCl. *J. Aerosol Sci.* **1989**, *20*, 1167–1170.
32. Keene, W.C.; Pszenny, A.A.P.; Jacob, D.J.; Duce, R.A.; Galloway, J.N.; Schultz-Tokos, J.J.; Sievering, H.; Boatman, J.F. The geochemical cycling of reactive chlorine through the marine troposphere. *Glob. Biogeochem. Cycles* **1990**, *4*, 407–430.
33. Knipping, E.M. Modeling Cl_2 formation from aqueous NaCl particles: Evidence for interfacial reactions and importance of Cl_2 decomposition in alkaline solution. *J. Geophys. Res.* **2002**, *107*, doi:10.1029/2001JD000867.
34. George, I.J.; Abbatt, J.P.D. Heterogeneous oxidation of atmospheric aerosol particles by gas-phase radicals. *Nat. Chem.* **2010**, *2*, 713–722.
35. Kercher, J.P.; Riedel, T.P.; Thornton, J.A. Chlorine activation by N_2O_5: Simultaneous, in situ detection of $ClNO_2$ and N_2O_5 by chemical ionization mass spectrometry. *Atmos. Measu. Tech.* **2009**, *2*, 193–204.
36. Thornton, J.A.; Abbatt, J.P.D. N_2O_5 reaction on submicron sea salt aerosol: Kinetics, products, and the effect of surface active organics. *J. Phys. Chem. A* **2005**, *109*, 10004–10012.
37. Osthoff, H.D.; Roberts, J.M.; Ravishankara, a. R.; Williams, E.J.; Lerner, B.M.; Sommariva, R.; Bates, T.S.; Coffman, D.; Quinn, P.K.; Dibb, J.E.; *et al.* High levels of nitryl chloride in the polluted subtropical marine boundary layer. *Nat. Geosci.* **2008**, *1*, 324–328.
38. Roberts, J.M.; Osthoff, H.D.; Brown, S.S.; Ravishankara, A.R.; Coffman, D.; Quinn, P.; Bates, T. Laboratory studies of products of N_2O_5 uptake on Cl-containing substrates. *Geophys. Res. Lett.* **2009**, *36*, doi:10.1029/2009GL040448.

39. Sarwar, G.; Simon, H.; Bhave, P.; Yarwood, G. Examining the impact of heterogeneous nitryl chloride production on air quality across the United States. *Atmos. Chem. Phys.* **2012**, *12*, 6455–6473.
40. Simon, H.; Kimura, Y.; McGaughey, G.; Allen, D.T.; Brown, S.S.; Coffman, D.; Dibb, J.; Osthoff, H.D.; Quinn, P.; Roberts, J.M. Modeling heterogeneous $ClNO_2$ formation, chloride availability, and chlorine cycling in Southeast Texas. *Atmos. Environ.* **2010**, *44*, 5476–5488.
41. Simon, H.; Kimura, Y.; McGaughey, G.; Allen, D.T.; Brown, S.S.; Osthoff, H.D.; Roberts, J.M.; Byun, D.; Lee, D. Modeling the impact of $ClNO_2$ on ozone formation in the Houston area. *J. Geophys. Res.* **2009**, *114*, doi:10.1029/2008JD010732.
42. Sarwar, G.; Simon, H.; Xing, J.; Mathur, R. Importance of tropospheric $ClNO_2$ chemistry across the Northern Hemisphere. *Geophys. Res. Lett.* **2014**, *41*, 4050–4058.
43. Roberts, J.M.; Osthoff, H.D.; Brown, S.S.; Ravishankara, A.R. N_2O_5 oxidizes chloride to Cl_2 in acidic atmospheric aerosol. *Science* **2008**, *321*, 1059–1059.
44. Thomas, J.L.; Jimenez-Aranda, A.; Finlayson-Pitts, B.J.; Dabdub, D. Gas-phase molecular halogen formation from NaCl and NaBr aerosols: when are interface reactions important? *J. Phys. Chem. A* **2006**, *110*, 1859–1867.
45. Phillips, G.J.; Tang, M.J.; Thieser, J.; Brickwedde, B.; Schuster, G.; Bohn, B.; Lelieveld, J.; Crowley, J.N. Significant concentrations of nitryl chloride observed in rural continental Europe associated with the influence of sea salt chloride and anthropogenic emissions. *Geophys. Res. Lett.* **2012**, *39*, doi:10.1029/2012GL051912.
46. Thornton, J.A.; Kercher, J.P.; Riedel, T.P.; Wagner, N.L.; Cozic, J.; Holloway, J.S.; Dubé, W.P.; Wolfe, G.M.; Quinn, P.K.; Middlebrook, A.M.; *et al.* A large atomic chlorine source inferred from mid-continental reactive nitrogen chemistry. *Nature* **2010**, *464*, 271–274.
47. Mielke, L.H.; Furgeson, A.; Osthoff, H.D. Observation of $ClNO_2$ in a mid-continental urban environment. *Environ. Sci. Technol.* **2011**, *45*, 8889–8896.
48. Behnke, W.; George, C.; Scheer, V.; Zetzsch, C. Production and decay of $ClNO_2$ from the reaction of gaseous N_2O_5 with NaCl solution: Bulk and aerosol experiments. *J. Geophys. Res.* **1997**, *102*, 3795–3804.
49. Behnke, W.; Krüger, H.-U.; Scheer, V.; Zetzsch, C. Formation of atomic Cl from sea spray via photolysis of nitryl chloride: Determination of the sticking coefficient of N_2O_5 on NaCl aerosol. *J. Aerosol Sci.* **1991**, *22*, S609–S612.
50. Frenzel, A.; Scheer, V.; Sikorski, R.; George, C.; Behnke, W.; Zetzsch, C. Heterogeneous interconversion reactions of $BrNO_2$, $ClNO_2$, Br_2, and Cl_2. *J. Phys. Chem. A* **1998**, *102*, 1329–1337.
51. Schweitzer, F.; Mirabel, P.; George, C. Multiphase chemistry of N_2O_5, $ClNO_2$, and $BrNO_2$. *J. Phys. Chem. A* **1998**, *102*, 3942–3952.
52. Bertram, T.H.; Thornton, J.A. Toward a general parameterization of N_2O_5 reactivity on aqueous particles: The competing effects of particle liquid water, nitrate and chloride. *Atmos. Chem. Phys. Discuss.* **2009**, *9*, 15181–15214.
53. Mielke, L.H.; Stutz, J.; Tsai, C.; Hurlock, S.C.; Roberts, J.M.; Veres, P.R.; Froyd, K.D.; Hayes, P.L.; Cubison, M.J.; Jimenez, J.L.; *et al.* Heterogeneous formation of nitryl chloride and its role as a nocturnal NO_x reservoir species during CalNex-LA 2010. *J. Geophys. Res. Atmos.* **2013**, *118*, 10638–10652.

54. Tham, Y.J.; Yan, C.; Xue, L.; Zha, Q.; Wang, X.; Wang, T. Presence of high nitryl chloride in Asian coastal environment and its impact on atmospheric photochemistry. *Chin. Sci. Bull.* **2013**, *59*, 356–359.
55. Riedel, T.P.; Wagner, N.L.; Dubé, W.P.; Middlebrook, A.M.; Young, C.J.; Öztürk, F.; Bahreini, R.; VandenBoer, T.C.; Wolfe, D.E.; Williams, E.J.; *et al.* Chlorine activation within urban or power plant plumes: Vertically resolved $ClNO_2$ and Cl_2 measurements from a tall tower in a polluted continental setting. *J. Geophys. Res. Atmos.* **2013**, *118*, 8702–8715.
56. National Aeronautics and Space Administration. Deriving Information on Surface Conditions from Column and Vertically Resolved Observations Relevant to Air Quality (DISCOVER-AQ). Available online: http://discover-aq.larc.nasa.gov/ (accessed on 31 August 2015).
57. Ng, N.L.; Herndon, S.C.; Trimborn, a.; Canagaratna, M.R.; Croteau, P.L.; Onasch, T.B.; Sueper, D.; Worsnop, D.R.; Zhang, Q.; Sun, Y.L.; *et al.* An Aerosol Chemical Speciation Monitor (ACSM) for routine monitoring of the composition and mass concentrations of ambient aerosol. *Aerosol Sci. Technol.* **2011**, *45*, 780–794.
58. Finley, B.D.; Saltzman, E.S. Observations of Cl_2 , Br_2 , and I_2 in coastal marine air. *J. Geophys. Res.* **2008**, *113*, 1–14.
59. Jordan, C.E.; Pszenny, A.A.P.; Keene, W.C.; Cooper, O.R.; Deegan, B.; Maben, J.; Routhier, M.; Sander, R.; Young, A.H. Origins of aerosol chlorine during winter over north central Colorado, USA. *J. Geophys. Res. Atmos.* **2015**, *120*, 678–694.
60. Young, A.H.; Keene, W.C.; Pszenny, A.A.P.; Sander, R.; Thornton, J.A.; Riedel, T.P.; Maben, J.R. Phase partitioning of soluble trace gases with size-resolved aerosols in near-surface continental air over northern Colorado, USA, during winter. *J. Geophys. Res. Atmos.* **2013**, *118*, 9414–9427.
61. Pratt, K.A.; Prather, K.A. Aircraft measurements of vertical profiles of aerosol mixing states. *J. Geophys. Res. Atmos.* **2010**, *115*, 1–10.
62. Hildebrandt Ruiz, L.; Yarwood, G.; Koo, B.; Heo, G. Quality assurance project plan project 14-024—Sources of organic particulate matter in Houston: Evidence from DISCOVER-AQ data modeling and experiments. Available online: http://aqrp.ceer.utexas.edu/projectinfoFY14_15%5C14-024%5C14-024%20QAPP.pdf (accessed on 31 August 2015).
63. Draxler, R.R.; Hess, G. Description of the HYSPLIT_4 Modeling System. Available online: https://ready.arl.noaa.gov/HYSPLIT.php; 2010 (accessed on 31 August 2015).
64. Yarwood, G.; Jung, J.; Whitten, G.Z.; Heo, G.; Mellberg, J.; Estes, M. Updates to the Carbon Bond mechanism for version 6 (CB6). In Proceedings of the 9th Annual CMAS Conference, Chapel Hill, NC, USA, 11–13 October 2010; pp. 1–4.
65. Yarwood, G.; Rao, S. *Updates to the Carbon Bond Chemical Mechanism: CB05*; RT-0400675; Final report to the US EPA; US EPA: Washington, DC, USA, 2005.
66. Tanaka, P.L.; Allen, D.T.; McDonald-Buller, E.C.; Chang, S.; Kimura, Y.; Mullins, C.B.; Yarwood, G.; Neece, J.D. Development of a chlorine mechanism for use in the carbon bond IV chemistry model. *J. Geophys. Res.* **2003**, *108*, doi: 10.1029/2002JD002432.
67. Carter, W.P.L.; Luo, D.; Malkina, I.L.; Pierce, J.A. Environmental Chamber Studies of Atmospheric Reactivities of Volatile Organic Compounds: Effects of Varying Chamber and Light Source; 1995. Availavle online: https://www.cert.ucr.edu/~carter/pubs/explrept.pdf (accessed on 31 August 2015).

68. Sokolov, O.; Hurley, M.D.; Wallington, T.J.; Kaiser, E.W.; Platz, J.; Nielsen, O.J.; Berho, F.; Rayez, M.T.; Lesclaux, R. Kinetics and mechanism of the gas-phase reaction of Cl atoms with benzene. *J. Phys. Chem. A* **1998**, *102*, 10671–10681.
69. Wingenter, O.W.; Blake, D.R.; Blake, N.J.; Sive, B.C.; Rowland, F.S.; Atlas, E.; Flocke, F. Tropospheric hydroxyl and atomic chlorine concentrations, and mixing timescales determined from hydrocarbon and halocarbon measurements made over the Southern Ocean. *J. Geophys. Res.* **1999**, *104*, 21,819–21,828.
70. Bertram, T.H.; Kimmel, J.R.; Crisp, T.A.; Ryder, O.S.; Yatavelli, R.L.N.; Thornton, J.A.; Cubison, M.J.; Gonin, M.; Worsnop, D.R. A field-deployable, chemical ionization time-of-flight mass spectrometer. *Atmos. Meas. Tech.* **2011**, *4*, 1471–1479.
71. Yatavelli, R.L.N.; Lopez-Hilfiker, F.; Wargo, J.D.; Kimmel, J.R.; Cubison, M.J.; Bertram, T.H.; Jimenez, J.L.; Gonin, M.; Worsnop, D.R.; Thornton, J.A. A chemical ionization high-resolution time-of-flight mass spectrometer coupled to a Micro Orifice Volatilization Impactor (MOVI-HRToF-CIMS) for analysis of gas and particle-phase organic species. *Aerosol Sci. Technol.* **2012**, *46*, 1313–1327.
72. Lee, B.H.; Lopez-Hilfiker, F.D.; Mohr, C.; Kurtén, T.; Worsnop, D.R.; Thornton, J.A. An iodide-adduct high-resolution time-of-flight chemical-ionization mass spectrometer: Application to atmospheric inorganic and organic compounds. *Environ. Sci. Technol.* **2014**, *48*, 6309–6317.
73. Aljawhary, D.; Lee, A.K.Y.; Abbatt, J.P.D. High-resolution chemical ionization mass spectrometry (ToF-CIMS): Application to study SOA composition and processing. *Atmos. Meas. Tech.* **2013**, *6*, 3211–3224.
74. Slusher, D.L.; Huey, L.G.; Tanner, D.J.; Flocke, F.M.; Roberts, J.M. A Thermal Dissociation-Chemical Ionization Mass Spectrometry (TD-CIMS) technique for the simultaneous measurement of peroxyacyl nitrates and dinitrogen pentoxide. *J. Geophys. Res.* **2004**, *109*, doi:10.1029/2004JD004670.
75. Zheng, W.; Flocke, F.M.; Tyndall, G.S.; Swanson, A.; Orlando, J.J.; Roberts, J.M.; Huey, L.G.; Tanner, D.J. Characterization of a thermal decomposition chemical ionization mass spectrometer for the measurement of Peroxy Acyl Nitrates (PANs) in the atmosphere. *Atmos. Chem. Phys.* **2011**, *11*, 6529–6547.
76. Fuchs, H.; Dube, W.P.; Ciciora, S.J.; Brown, S.S. Determination of inlet transmission and conversion efficiencies for in situ measurements of the nocturnal nitrogen oxides, NO_3, N_2O_5 and NO_2, via pulsed cavity ring-down spectroscopy. *Anal. Chem.* **2008**, *80*, 6010–6017.